The role of sediment gravity flows on the morphological development of a large submarine canyon (Taiwan Canyon), northeast South China Sea

Wei Li [1, 2, 3, 4]*, Shuang Li [1, 2, 3, 4], Tiago M. Alves [5], Michele Rebesco [6]

[1] CAS Key Laboratory of Ocean and Marginal Sea Geology, South China Sea Institute of Oceanology, Chinese Academy of Sciences, Guangzhou 510301, P.R. China

[2] Southern Marine Science and Engineering Guangdong Laboratory (Guangzhou), 511458, P.R. China

[3] Innovation Academy of South China Sea Ecology and Environmental Engineering, Chinese Academy of Sciences, Guangzhou 510301, P.R. China

[4] University of Chinese Academy of Sciences, Beijing 100049, P.R. China

[5] 3D Seismic Lab. School of Earth and Ocean Sciences, Cardiff University, Main Building, Park Place, Cardiff, CF10 3AT, United Kingdom

[6] Istituto Nazionale di Oceanografia e di Geofisica Sperimentale (OGS), Borgo Grotta Gigante 42/C, Sgonico, 34010 Trieste, Italy

*Corresponding author: Dr. Wei Li (wli@scsio.ac.cn)

ABSTRACT

High-resolution multibeam bathymetric and multichannel seismic data are used to investigate the morphology of a submarine canyon (Taiwan Canyon), and surrounding strata, in the northeast South China Sea. This submarine canyon shows two main branches at its head, and changes its orientation from NW-SE to E-W due to the effect of a tectonically active seamount. The asymmetry of the submarine canyon's banks in its middle reach is due to the combined action of recurrent slope instability and turbidity currents. Two fields of sediment waves were also identified in the study area. Field 1 is located on the southwest levee of the canyon and is fed by turbidity currents from one of its branches, being also associated with marked hydraulic jumps. Field 2 is observed in the southern bank of the lower canyon reach and was formed by the overspill of turbidity currents within the

Taiwan Canyon due to the effect of inertial centrifugal forces. Turbidity currents sourced from Dongsha Channel also contributed to forming Field 2. Importantly, trains of plunge pools have been identified along the thalweg of the lower canyon reach, generated by turbidity currents deriving from the submarine canyons in the north of the Taiwan Canyon. Our results not only provide a very detailed account of submarine bedforms within and around a large submarine canyon, but also contribute to a better understand of their origin and development. The high-resolution bathymetric and seismic data in this work reveal how gravity flows can drive erosion and deposition in submarine canyons.

Keywords: South China Sea; Taiwan Canyon; slope failures; turbidity currents; sediment waves; plunge pools.

INTRODUCTION

Sediment gravity flows, usually occurring as submarine landslides and turbidity currents, are ubiquitous on both passive and active continental margins (Talling et al., 2012). Sub-marine landslides can generate enormous turbidity currents and mass-transport deposits, or MTDs (Nisbet and Piper, 1998). They both play significant roles in eroding continental shelves and slopes, leading to the incision of submarine canyons while transporting large volumes of sediment into deep-sea environments (Canals et al., 2006; Talling et al., 2012). In addition, sediment gravity flows can generate widespread seafloor bedforms within and around submarine canyons, including vast fields of sediment waves (Kostic, 2014; Symons et al., 2016; Normandeau et al., 2018), seafloor scours (Lamb et al., 2008; Covault et al., 2014), troughs and plunge pools (Paull et al., 2011; Schnyder et al., 2018).

Large submarine canyons have been documented on the northern South China Sea margin, where sediment gravity flows play a vital role in their morphological development. Key examples are the Central Canyon in the Qiongdongnan Basin (Gong et al., 2011; Li et al., 2013), the Pearl River Canyon (Ding et al., 2013; Wang et al., 2017) and the multiple slope-confined canyons of the Pearl River Mouth Basin (Gong et al., 2013) (Fig. 1). The Central Canyon was formed by the incision of large-scale gravity flows (slumps, debris flows and turbidity currents), which started in the Late Miocene (5.5 Ma) (Li et al., 2013). Two main phases of Quaternary mass-wasting have been recognised in the middle segment of the Pearl River Canyon, indicating that MTDs play a significant role in its development (Wang et al., 2017). There is also a clear asymmetry in the sub-linear, slope-confined canyons in the Pearl River Month Basin, as shown by their steep eastern walls and stepped, curved western walls sculpted by slumps and slides (Ding et al., 2013; He et al., 2014). Yin et al. (2019) link the asymmetry of these submarine canyons to contour currents, as well as to turbidity currents.

The Taiwan Canyon (also called South Taiwan Shoal Canyon or Taiwan Bank Canyon) is one of the largest submarine canyons on the northeastern South China Sea margin, reaching a total length of ~220 km (Ding et al., 2010; Xu et al., 2014; Zhong et al., 2015) (Fig. 1). Using two-dimensional seismic and bathymetric data, Ding et al. (2010) revealed that the Taiwan Canyon was initiated in the Middle Miocene, and tectonic structures (i.e. transform fault and seamount) have affected its orientation since then. The origin and development of Taiwan Canyon were also investigated, and high sediment supply, frequent gravity sliding (slumping) and faulting activities were considered as the main controlling factors (Xu et al., 2014). Four fields of sediment waves are reported on the northeast South China Sea and three of them are located around the Taiwan Canyon (Gong et al., 2012; Kuang et al., 2014; Gong et al., 2015; Yin et al., 2015). Recent studies have documented the complex morphology of scours along its thalweg, interpreting them as cyclic steps resulting from the interaction of supercritical turbidity currents with the seafloor (Zhong et al., 2015).

This paper focuses on the sediment gravity flows of the northeast South China Sea and their roles on the morphological development of the Taiwan Canyon. Sediment gravity flows occur frequently within and around the Taiwan Canyon due to the frequent earthquakes that affect the Manila Trench (Liu et al., 2013). Seasonal typhoons are also capable of triggering turbidity currents in this region (Zhang et al., 2018). This study investigates the morphological features within and around the Taiwan Canyon in a greater detail than previous publications (Figs. 1 and 2). Though sediment wave fields around the Taiwan Canyon have been recognised in previous work (Gong et al., 2012; Kuang et al., 2014), their origin and formation mechanisms are still poorly understood. This paper reveals for the first time that levees in the middle reach of Taiwan Canyon are asymmetric and that a narrow (~1.6 km wide), elongated (~42 km long) trough with a W-E orientation occurs in the lower reach of Taiwan Canyon. This latter trough has not been identified in the published literature. Hence, a comprehensive analysis of submarine features and structures within and around the Taiwan Canyon is presented in this work with the ultimate aim of:

1) Investigating the factors controlling the asymmetry of the middle reach of the Taiwan Canyon;
2) Determining the processes responsible for the formation of sediment waves around the Taiwan Canyon;
3) Discussing how gravity flows can form erosional depressions in the lower reach of Taiwan Canyon.

GEOLOGICAL SETTING

The South China Sea (SCS) is a wedge-shaped marginal sea whose oceanic crust is wider in its eastern part, narrowing down towards the southwest (Taylor and Hayes, 1983; Hsu et al., 2004).

Passive rifting in the SCS was initiated in the Late Cretaceous by N-S crustal extension (Wang et al., 2006). A Late Oligocene to Middle Miocene phase of seafloor spreading followed the initial stages of continental rifting, and was associated with progressive continental breakup along the SCS (Taylor and Hayes, 1983; Zhao et al., 2016).

The study area is located to the northwest of the Taixinan Basin at a water depth of 200 m to 3500 m, in the northeast SCS (Figs. 1 and 2a). The Taiwan Canyon started to form in the Late Miocene (Ding et al., 2010; Xu et al., 2014; Liao et al., 2016). During the Pliocene, the Taiwan Canyon served as the main sediment conduit transporting terrestrial coarse-grained sediment onto deep-water depocenters (Liao et al., 2016), shifted eastwards to converge with the Manila Trench during the late Pleistocene (Liao et al., 2016). At this time, the ancient Hanjiang River flowed through the present-day continental shelf to transport fluvial sediments directly to the Taiwan Canyon (Xu et al., 2014).

A left-lateral transform fault, called the Luzon-Ryukyu Transform Fault (LRTF), is located in the southern part of the Taiwan Canyon (Fig. 2b). The LRTF is revealed by changes in the trend of magnetic anomalies on the ocean floor, as well as changes in seafloor bathymetry and basement relief (Sibuet et al., 2002; Hsu et al., 2004). The fault connects the former southeast-dipping Manila Trench with the northwest-dipping Ryukyu Trench. In the Early Miocene, the LRTF became inactive due to the formation of the Luzon Arc and onset of seafloor spreading in the eastern SCS between 20 and 18 Ma (Hsu et al., 2004). In addition to the LRTF, a seamount lies in the northwestern region of the Taiwan Canyon (Fig. 2). This seamount was formed during the Early Miocene (21-22 Ma) as revealed by the $^{40}Ar/^{39}Ar$ dating of its alkali basaltic rocks (Wang et al., 2012).

DATA AND METHODS

Bathymetric and seismic data

Multibeam bathymetric and multichannel seismic data are used as the primary datasets in this work. These bathymetric data were acquired onboard the R/V SONNE during the joint Chinese-German Cruise 177, June 2004, using a SIMRAD EM120 multi-beam echo-sounder system. The horizontal and vertical resolutions of the bathymetric data are ~100 m and 3-6 m, respectively. The multibeam bathymetric data were imported and analysed in Global Mapper®.

Multichannel seismic data are used to characterize near-seafloor bedforms around the Taiwan Canyon. Two long seismic-reflection profiles (MGL0905-05 (~70 km) and MGL0905-10 (~41 km)), acquired as part of the Taiwan Integrated Geodynamic Research (TAIGER) project, are also used in this work together with an additional two-dimensional (2D) multichannel seismic profile acquired by the South China Sea Institute of Oceanology, Chinese Academy of Sciences, in May 2019 (Fig. 2). The frequency bandwidth of this latter seismic profile is 30-45 Hz, providing an average vertical resolution of 11-17 m for shallow strata. The seismic profile was acquired by 1800 m-long streamer with 144-channels and spaced 12.5 m (Fig. 2). The seismic profile was processed using RadExpro® and interpreted on Geoframe®.

Calculations of turbidity current properties

The flow properties of turbidity currents flowing through the sediment wave fields were calculated based on the morphological parameters of the sediment waves identified in seismic and bathymetric data. These morphological parameters include the wavelength and the slope gradient of the lee and stoss sides of sediment waves, which are used in several equations to calculate:

1) the internal Froude number (F_i) of turbidity currents using the slope gradient (α), drag

coefficient at the bed (C_f), and entrainment coefficient at the upper interface (e), as represented by Equation (1);

2) the flow thickness (h) using the relationship between wavelength (L) and the internal Froude number (F_i) in Equation (2);

3) the velocity of sediment waves in the stoss and lee sides using Δρ (grain density - density of turbidity currents/seawater density), C (the volume concentration), g (gravitational acceleration), internal Froude number (F_i) and flow thickness (h).

$$F_i^2 = \frac{\sin(\alpha)}{C_f + e} \tag{1}$$

$$h = \frac{L}{2\pi F_i^2} \tag{2}$$

$$u^2 = \Delta\rho\ CghF_i^2 \tag{3}$$

where F_i is the internal Froude number of turbidity currents, and α is slope gradient of sediment waves. Suggested values for the drag coefficient C_f of turbidity currents range from 3.5×10^{-3} to 4×10^{-3} (Bowen et al., 1984). The lowest value of $3.5x10^{-3}$ is more applicable to unconfined flows (Wynn et al., 2000). The entrainment coefficient e for most turbidity currents varies between 5×10^{-4} and 6×10^{-3}, while sediment concentration (C) is a dimensionless number ranging from 5×10^{-5} to 5×10^{-4} (Piper and Savoye, 1993). The parameter g represents the gravitational acceleration, considered to be 9.81 m/s^2.

This work calculated the Froude numbers of circular depressions within the Taiwan Canyon, before and after hydraulic jumps, using Equations (4) and (5).

$$Fr_1 = \frac{U}{\sqrt{\Delta\rho Cgh}} \tag{4}$$

$$F_{r_2} = \frac{2^{1.5} F_{r_1}}{(\sqrt{1+8{F_{r_1}}^2}-1)^{1.5}} \quad (5)$$

where the sediment concentration (C) is the volume sediment concentration, g is the gravitational acceleration (9.81 m/s^2). The parameter h is the flow depth of turbidity currents and U represents the velocity of turbidity currents. Δρ (sediment density - density of turbidity currents/seawater density).

RESULTS

Morphological evolution of the Taiwan Canyon

The Taiwan Canyon is observed at a water depth ranging from 500 m to 3500 m (Fig. 2a). The Taiwan Canyon is approximately 220 km long and 6 to 12 km wide. In bathymetric data, Branch 1 is located in the northern part of the Taiwan Canyon at a water depth between 2000 m to 2500 m, while branch 2 is oriented NW-SE and occurs at a water depth of 2100 to 2500 m (Fig. 2). Branch 1 is 7 km wide and ~42 km long, while branch 2 is 6 km wide and 40 km long (Fig. 2a).

The middle reach of the Taiwan Canyon is ~80 km long and is observed at a water depth of 2500 m to 3125 m. Here, its banks are asymmetric in both their height and slope gradient (Figs. 3 and 4). The southwest bank of the Taiwan Canyon is steeper than its northeast counterpart; the slope gradient of the southwest bank ranges from 6.5° to 13°, whereas it ranges from 1° to 2° on the northeast bank (Figs. 3b and 4b). Moreover, the southwest bank of the Taiwan Canyon is higher than its northeast counterpart (~ 230 m and 300 m high, respectively) (Figs. 3b and 4b). Along the middle reach of the Taiwan Canyon, MTDs are presented on the seismic profiles, appearing as discontinuous, transparent reflections (Figs. 3c and 4c). These MTDs occur along the base of the continental slope in Pliocene and Pleistocene strata (Liao et al., 2016), indicating complex cut-and-fill processes during the development of Taiwan Canyon.

The lower reach of the Taiwan Canyon is ~60 km long and occurs at a water depth of 3125 m to 3500 m (Fig. 2a). The Taiwan Canyon changes its orientation from NW-SE to nearly E-W at a water depth of 3070 m (Fig. 2). A seamount is located to the southwest part of the canyon at a water depth of 2750 m. The seamount is 1200 m high and 6-8 km wide, spanning ~70 km^2 of the continental slope (Fig. 2).

Sediment waves fields around the Taiwan Canyon

Two fields of sediment waves are observed around the Taiwan Canyon. Field 1 spans the southwest levee in the middle reach of Taiwan Canyon at a water depth of 2250 m to 2840 m, with a slope gradient of 0.5° on average (Figs. 2a and 5c). These sediment waves cover ~510 km^2 of the levee and their dimensions (wavelengths and wave heights) become smaller with increasing water depth (Figs. 2a, 5c and 6b). The wavelength of sediment waves in Field 1, from head to tail, ranges from 1.2 km to 3.7 km and show wave heights of 30 m to 47 m. The slope gradient ranges from 0.43° to 1.78° on the stoss sides of Field 1, and 1.09° to 2.49° on the observed lee sides (Table 1). The crests of sediment waves are bifurcated and their orientation approaches NW-SE (Fig. 2). The seismic reflections within the sediment waves are continuous and can be traced from one wave to another (Fig. 5c). Discrete sediment waves show asymmetrical geometries with a long and thicker upslope flank but a short and thinner downslope flank, and their crests display a trend of upslope migration (Fig. 5c). This work estimates the velocities of turbidity currents flowing through Field 1 as comprising V_{stoss} from 2.16 m/s to 3.31 m/s and V_{lee} between 2.17 m/s and 3.4 m/s, based on Equations (1) - (3) (Table 1).

Field 2 is located in the southern side of the Taiwan Canyon at a water depth between 3150 m to 3500 m (Fig. 2a). Here, slope gradient reaches 0.57° on average, but only the northern part of the

Field 2 is fully imaged by our data set, covering a total area 870 km^2. These sediment waves are oblique to the orientation of the Taiwan Canyon and reveal a NW–SE orientation (Figs. 2, 5b and 7b). Sediment waves show asymmetrical profiles in cross-section and marked upslope-migrating, sinuous, bifurcate crests (Fig. 7b). These waves crests develop parallel in two trains with a E-W direction. Waves in Field 2 have relatively large dimensions, with wavelengths ranging from 1.5 km to 5.4 km and have wave heights ranging from 50 m to 110 m.

Trough along the Taiwan canyon thalweg

Troughs are narrow, elongated depressions on the seafloor with flat bottoms and steep flanks (Heap and Harris, 2008). In our study area, a new trough is identified in the lower reach of the Taiwan Canyon at a water depth from 3300 m to 3500 m, where the slope gradient is 0.3° on average (Figs. 2a and 8). It extends for ~44 km with an E-W orientation, and has a width of ~1.6 km, covering about 72 km^2 of the continental slope (Fig. 8c). This trough is close to the north bank of the lower reach of the Taiwan Canyon, and sediment waves are located further to the north (Figs. 8a, 8b and 9a). It has an incision depth of ~100 m on average, and shows several undulations in cross-section view and closed circular-shaped depressions in plan view (Figs. 8a and 8c). These depressions are 1.38 km to 3.86 km in diameter and 62 m to 119.1 m in height (Fig. 8c and Table 2). Moreover, marked differences in slope gradient can be observed on the walls of the lower reach of the Taiwan Canyon (Figs. 9b and 9d). The slope gradients of the northern canyon wall of these depressions range from 6.3° to 12.4°, while they vary from 3.2° to 14.3° on the southern canyon wall (Table 2).

DISCUSSION

Controls on the asymmetry of the middle reach of Taiwan canyon

Asymmetric submarine canyons have been widely observed when analyzing slope gradient and the height of canyon banks on cross-sectional bathymetric profiles (Mountjoy et al., 2009; Micallef et al., 2014). These asymmetric canyons have been suggested to result from regional tectonics (Dantec et al., 2010; Micallef et al., 2012), the effect of the Coriolis force (Cossu et al., 2010; Cossu et al., 2015), gravity flows (Keevil et al., 2007; Arzola et al., 2008) and contour currents acting on the continental slope (Fonnesu et al., 2020; Miramontes et al., 2020). In the study area, a prominent asymmetry in the Taiwan Canyon is documented not only by the recorded difference in its bank height, but also by analyzing slope gradients in its middle reach (Figs. 3b and 4b). Several potential controls on the asymmetry of the middle reach of Taiwan Canyon are discussed below.

Local tectonic structures such as folds and faults directly affect the location, alignment and geometry of many a submarine canyon (Dantec et al., 2010; Micallef et al., 2014). Several researchers have proposed the southwest levee of the middle reach of Taiwan Canyon to be part of a major transform plate boundary, the Luzon-Ryukyu Transform Fault (LRTF) (Sibuet et al., 2002; Yeh et al., 2004; Hsu et al., 2004). It appears that the orientation of the Taiwan Canyon is parallel to the Luzon-Ryukyu Transform Fault (LRTF). However, the Luzon-Ryukyu Transform Fault cannot be clearly identified on the seismic profiles across the Taiwan Canyon, and there is also no obvious fault close to the southwest bank of this canyon (Figs. 3 and 4). A series of normal faults occur only in much deeper strata (4.5 s-5.8 s TWTT), not influencing the asymmetry of the middle reach of Taiwan canyon (Figs. 3a and 4a). Therefore, this study proposes that regional tectonics affected the orientation of Taiwan Canyon but did not control the asymmetry observed in its middle reach.

In the Northern Hemisphere, the Coriolis force laterally deflects turbidity currents so that both their density interface and downstream velocity maxima are deflected to the right-hand side of submarine canyons in a downstream direction (Cossu et al., 2010). This shift in flow orientation can change the loci of erosion and deposition on continental slopes, and consequently impose differences in canyon bank height and slope gradient (Cossu and Wells, 2013; Cossu et al., 2015). The ratio between the Coriolis force and the inertial force of gravity flows in submarine canyons is represented by the Rossby number (Cossu et al., 2015).

Turbidity currents flowing southeast along the Taiwan Canyon are affected by the Coriolis force, resulting in enhanced erosion and therefore larger slope gradients in the southwest side of its middle reach. However, the Coriolis force may not impose great differences in canyon bank height due to the large Rossby number ($|Ro|>10$) recorded in low latitude areas (Cossu et al, 2010). In our study area, at a latitude of 21°N, the Rossby number ranges from 10 to 20, suggesting that the Coriolis force is not the main reason for the difference in canyon bank height recorded in the middle reach of the Taiwan Canyon.

Gravity flows such as submarine landslides are ubiquitous in deep-sea environments, and are the dominant processes eroding the continental slope and enlarging submarine canyons (Pratson and Coakley, 1996). Recurrent MTDs are identified in the northeast overbank of the middle reach of Taiwan Canyon (Figs. 3b and 4b); they are relatively younger than the Taiwan Canyon (Liao et al., 2016). The presence of stacked MTDs indicates that the northeast bank of Taiwan Canyon was eroded by slope failures originating from the area to the northeast (Fig. 8). This leads to the differences in canyon bank height in the middle reach of the Taiwan Canyon.

The simultaneous interaction of contour and turbidity currents on continental slopes can result in asymmetric canyon-levee systems (Gong et al., 2018; Fonnesu et al., 2020; Miramontes et al., 2020), especially in the zones where the downslope turbidity currents have velocities of 2 m/s or less, and where submarine channels are not deeply incised (Miramontes et al., 2020). The velocity of turbidity currents in the middle reach of Taiwan Canyon range from 4-10 m/s (Zhong et al., 2015), values that are 40-100 times larger than that of contour currents (~15 cm/s in average), as documented by Zhao et al. (2016) in the same area. For one thing, contour currents may not have a marked effect on the deflection of turbidity currents that flowing along the Taiwan Canyon towards southeast. In addition, the differences in water depth between the thalweg and southwest levee in the middle reach of Taiwan Canyon are ~300-400 m (Fig. 10), and such difference in levee height can prevent the overspill of turbidity currents from Taiwan Canyon.

In summary, this study suggests that erosion by recurrent slope failures to the northeast of the Taiwan Canyon is the main reason for the contrast in canyon bank heights (about 300 m on average). However, it also suggests that the observed differences in slope gradient on both banks of the Taiwan Canyon result mainly from the erosion of turbidity currents along the canyon which are heavily influenced by inertial centrifugal forces.

Mechanisms forming sediment waves around the Taiwan Canyon

Based on the interpretation of the multibeam bathymetric map and two-dimensional seismic profiles used in this study, two fields of sediment waves can be identified around the Taiwan Canyon (Fig. 2). The sediment waves in the lower reach of Taiwan Canyon are not the focus in this work as they have been proposed to be generated by unconfined turbidity currents flowing out of the West Penghu Canyon (Gong et al., 2012; Kuang et al., 2014). The formation of deep-water sediment waves has been attributed to multiple causes, including downslope turbidity currents (Wynn et al., 2002; Covault et al., 2014), along-slope contour (bottom) currents (Masson et al., 2002; Betzler et al., 2014), interactions between turbidity and contour currents (Normandeau et al., 2018) and submarine landslides (Hampton et al., 1996; Pope et al., 2018; Casalbore et al., 2020). In the following sections, the formation mechanisms of sediment waves in Fields 1 and 2 are analysed in detail.

Four key observations comprise key evidence to determine the formation mechanism of sediment waves in Fields 1 and 2.

(a) The crests of sediment waves in Fields 1 and 2 are parallel to the bathymetric contours (Fig. 2). Wynn et al. (2002) have proposed that crests of sediment waves formed by bottom currents are usually aligned at a low angle (typically 10°-50°) to the regional contours, while the crests of sediment waves generated by turbidity currents on slopes are normally slope-parallel. This indicates that the sediment waves in Fields 1 and 2 cannot be solely be produced by bottom currents.

(b) The wave crests are sinuous and bifurcate in plan view and they oblique to the orientation of Taiwan Canyon in its middle reach (Figs. 2a and 2b). In areas with good planform coverage most turbidity current sediment waves appear as linear features with varying degrees of sinuosity and/or bifurcation (Wynn et al., 2002; Symons et al., 2016), suggesting a turbidity current of origin for the sediment waves of Fields 1 and 2.

(c) The dimensions (wavelengths and wave heights) of sediment waves in Fields 1 and 2 decrease downslope in a gradual way (Figs. 5b, 5c and 6b). This is an important observation as sediment waves formed by turbidity currents are usually smaller in a downslope direction due to decreasing sediment supply and flow velocity downslope (Normark et al., 2002). In contrast, bottom current sediment waves are irregular with no consistent change in wave dimensions (Wynn et al., 2002).

(d) Discrete seismic reflections within the sediment waves are continuous and can be traced across the troughs from one wave to the next (Figs. 5b and 5c). Though seismic reflection patterns in the wave troughs can mimic fault planes in some cases, sediment waves formed by turbidity currents or bottom currents consist of continuous, parallel or sub-parallel reflections on both sides (Lee et al., 2002). In comparison, submarine landslides or creep folds show clear displacement along fault planes, especially in their troughs (Hill et al., 1982; Lee and Chough, 2001). This suggests that submarine landslides may not result in the formation of sediment waves in Fields 1 and 2. As discussed above, the sediment waves in Fields 1 and 2 are most likely generated by turbidity currents.

The crests of sediment waves are considered to align perpendicularly to the flow direction of turbidity currents (Wynn et al., 2002). The wave crests in Field 1 are W-E oriented and this reveals that turbidity currents were sourced from branch 1 of the Taiwan Canyon. Thus, turbidity current stripping is considered to have occurred from the main flow in the Taiwan Canyon. The stripped turbidity current flowed over the southern levee in a series of hydraulic jumps, leading to the generation of sediment waves in Field 1 (Fig. 8). Overspilling turbidity currents have been documented in the Monterey East Channel (Fildani et al., 2006) and the Eel Canyon offshore California (Lamb et al., 2008), where sediment waves are widely distributed. Additionally, the observed overspilling turbidity currents in Eel canyon and Monterey East Channel show gradually decrease in their velocities, and consequently result in the decrease in sediment waves' dimensions.

The wave crests in Field 2 are observed to be sinuous and bifurcate on the bathymetric map, which are more complex compared to those in Field 1 (Figs. 2a and 10). The bifurcation and sinuosity of wave crests suggest an interaction of turbidity currents from different areas (e.g. Wynn et al., 2000). Moreover, these wave crests extend in a N-S or NE-SW direction, and they develop as two trains (Figs. 2b and 10). This phenomenon indicates that turbidity currents may be derived from north or northwest of Field 2. Hence, two possible sources of turbidity currents are proposed that may overspill into this field of sediment waves. The most likely case is the overspill of turbidity currents from the Taiwan Canyon due to inertial centrifugal forces. In addition, the Dongsha Channel is located to the west of sediment waves in Field 2, and there might be turbidity currents flowing through this channel.

These flows are initially constrained within a confined environment, but rapidly become unconfined downslope and spread out over an extensive area.

Origin and development of plunge pools within the lower reach of Taiwan Canyon

Plunge pools are defined as a series of discrete depressions and occur at sharp changes in slope gradient exceeding 4° (Lee et al., 2002). They are widely distributed within submarine canyons on both active and passive continental margins (e.g. Betzler et al., 2014; Schnyder et al., 2018). In this study, several discontinuous depressions are located close to the north flank in the lower reach of Taiwan Canyon (Figs. 8b and 9a). The depth of these depressions is much larger than those documented in other area (Table 3). They show circular-shaped closed depressions on the contour map and are concave-shape in the cross section (Figs. 8a and c). Therefore, this study proposes that these depressions observed in the lower reach of Taiwan Canyon are plunge pools.

The formation of plunge pools in deep-sea environments is chiefly caused by: a) sediment-laden density flows ("impact pools"), b) erosion by contour currents or c) hydraulic jumps in turbidity currents ("hydraulic jump pools") (Lee et al., 2002). Plunge pools generated by sediment-laden density flows often have larger slope gradients in their upslope bank (> 20°) (Pratson et al., 2001; Lee et al., 2002). However, the plunge pools in our study are characterised by slope gradients from 6.3^{o} to 12.4 ^{o} on their northern flank, which is much smaller than the typical gradients of impact pools (Table 2 and Table 3). Thus, sediment-laden density flows should not be responsible for the generation of plunge pools in the study area. Depressions created by contour currents are generally wider than plunge pools, forming an elongate trough instead of a series of discrete depressions (Stow et al., 1998; Lee et al., 2002). In this study, the plunge pools are N-S orientated (Figs. 8b and 10), a direction perpendicular to the bottom currents flowing along the lower reach of Taiwan Canyon (Gong et al., 2012; Liu et al., 2016). This indicates that these plunge pools are unlikely to be formed by along-slope bottom currents.

The sharp change of calculated Froude numbers suggest that turbidity currents change their flow regime from supercritical to subcritical when passing over the bottom of plunge pools. Moreover, a sediment core collected on the southern edge of a Quaternary plunge pool indicates fine-to-medium grained sands and silts ranging in grain-size from 4Φ to 8Φ in the Krumbeinphi scale (Gong et al., 2012; Gong et al., 2015). These two lines of evidence suggest that plunge pools are most likely formed by hydraulic jumps of turbidity currents. There are two sources of turbidity currents that may flow through plunge pools, including the turbidity currents (towards east) within the Taiwan Canyon, and turbidity currents (towards south) from the northern bank of Taiwan Canyon. If the plunge pools were generated by turbidity currents within the Taiwan Canyon, they would overspill to the southeast due to the occurrence of the seamount (Fig. 2). They would be affected by the Coriolis force, resulting in enhanced erosion close to the south side of the lower reach of the Taiwan Canyon. These phenomena are inconsistent with the present of a series of plunge pools adjacently to the northern bank of Taiwan Canyon's lower reach. Thus, turbidity currents might be sourced from the northern bank (e.g. West Penghu Canyon) of the Taiwan Canyon.

IMPLICATIONS

Our results provide three main contributions towards a better understanding of sediment gravity flows (turbidity currents and submarine landslides) and their roles on the morphological development of submarine canyons.

Turbidity currents are one the most important but also one of the least documented sediment transport processes on Earth (Talling et al., 2007; Paull et al., 2018). They can strongly modify the seafloor morphology and generate various submarine bedforms (Talling et al., 2007; Meiburg and Kneller, 2010). Frequent turbidity currents with high velocity (5-8 m/s) have been documented on the northeastern South China Sea margin by in situ measurement (Zhang et al., 2018). In this study, the velocity of turbidity currents is still 3-4 m/s after overspilling the southwest levee in middle reach of Taiwan Canyon (~300-400 m), leading to the formation of sediment waves in Field 1 (Fig. 10). Several plunge pools are discovered in the lower reach of Taiwan Canyon. The origin and development of these plunge pools strongly suggests the powerful erosional ability of turbidity currents when entering the Taiwan Canyon. In contrast to the previous literature (Xu et al., 2014; Kuang et al., 2014; Yin et al., 2015), this study succeeds in reporting numerous morphological features (sediment waves and plunge pools) within and around the Taiwan Canyon to reveal the role of turbidity currents on their development.

The dimensions (wavelengths and wave heights) of sediment waves are mainly controlled by the hydraulic characteristics of turbidity currents (e.g. velocity, discharge and energy loss) (Wynn et al., 2002; Symons et al., 2016). Though sediment waves have been reported on the southwest levee of middle reach of Taiwan Canyon in pervious literature (e.g. Kuang et al., 2014; Zhong et al., 2015; Yin et al., 2015), this study conducts a quantitative analysis of their formation mechanism and proposes a schematic model for their development. This work contributes to a more complete understanding of flow dynamics in turbidity currents occurring around submarine canyons.

Submarine landslides can transport large volume of sediment from the continental slope to the deep ocean (Hampton et al., 1996; Nisbet and Piper, 1998; Pope et al., 2015) and they can largely affect the seafloor morphology by producing slide scars (Williams, 2016). The asymmetry of submarine canyons (i.e. the difference of height and slope gradient of canyon flank) have been suggested to be caused by regional tectonics (Micallef et al., 2012), the deflection of turbidity currents

(Cossu et al., 2015) and the interaction of turbidity currents and contour currents (Miramontes et al., 2020). In this work, the marked asymmetry in the middle reach of the Taiwan Canyon is first reported, and the huge difference recorded here in terms of canyon levee height (up to 400 m), differences rarely documented in other regions. The repeated submarine landslides have eroded the northeastern levee in the middle reach of Taiwan Canyon, resulting in the asymmetrical geometry of Taiwan Canyon in its middle reach. Our results provide a new case study and explanation related to the controlling factors on the asymmetry of submarine canyons.

CONCLUSIONS

High-resolution multibeam bathymetric and multichannel seismic data are used in this study to investigate the development and geomorphology of the Taiwan Canyon. The main conclusions are as follows:

(1) Seafloor bedforms include two fields of sediment waves (Fields 1 and 2) and a series of plunge pools identified within and around the Taiwan Canyon. A seamount is located in the southwest part of the Taiwan Canyon, resulting in changes in the orientation of this latter, from NW-SE to nearly W-E.

(2) Marked asymmetry is observed in the middle reach of the Taiwan Canyon. The southwest bank of the canyon is much higher than its northeast counterpart, showing an average height difference of up to 400 m. The southwest bank of the canyon reveals more erosion than the opposite bank.

(3) Recurrent slope failures sourced from the northeast side of the middle reach of the Taiwan Canyon are considered as the main reason for obvious difference in canyon bank heights. Variations in the erosion power of landslides and turbidity currents are due to the effect of the inertial centrifugal

forces.

(4) Sediment waves in Field 1 are related to turbidity currents sourced from branch 1 of the Taiwan Canyon. They are also associated with marked hydraulic jumps of ~300 m. The velocity of turbidity currents flowing through the stoss and lee sides of sediment waves ranges from 2.16 m/s to 3.31 m/s, and 2.17 m/s to 3.4 m/s, respectively.

(5) Three sources of turbidity currents are proposed to be responsible for the formation of sediment waves in Field 2. The most likely scenario is that the turbidity currents overspill the Taiwan Canyon due to inertial centrifugal forces. Turbidity currents from Dongsha Channel and submarine canyons in the north of Taiwan Canyon might also contribute to the generation of sediment waves in Field 2.

(6) Plunge pools are observed close to the northern bank of the Taiwan Canyon, and their formation is related to erosion imposed by turbidity currents sourcing from the submarine canyons in the north of Taiwan Canyon. The northern banks of plunge pools reveal steeper slope gradients than their opposite sides.

ACKNOWLEDGEMENTS

This work was financially supported by Guangdong Basic and Applied Basic Research Foundation (2020B1515020016), Key Special Project for Introduced Talents Team of Southern Marine Science and Engineering Guangdong Laboratory (Guangzhou) (GML2019ZD0104), National Natural Science Foundation of China (41706054 and 41876054) and National Natural Science Foundation of Guangdong Province (2020A1515010497). Dr. Wei Li is funded by the CAS Pioneer Hundred Talents Program. The editors (Dr. Ian Kane and Prof. Dr. Zhifei Liu), Dr. Chenglin Gong and two anonymous reviewers are thanked for their constructive comments. The data that support the findings of this study are available from the corresponding author upon reasonable request.

REFERENCES

Arzola, R.G., Wynn, R.B., Lastras, G., Masson, D.G. andWeaver, P.P.E. (2008) Sedimentary features and processes in the Nazaré and Setúbal submarine canyons, west Iberian margin. Marine Geology., 250, 64-88.

Betzler, C., Lindhorst, S., Eberli, G.P., Lüdmann, T., Möbius, J., Ludwig, J., Schutter, I., Wunsch, M., Reijmer, J.J.G. and Hübscher, C. (2014) Periplatform drift: The combined result of contour current and off-bank transport along carbonate platforms. Geology., 42, 871-874.

Bowen, A.J., Normark, W.R. and Piper, D.J.W. (1984) Modelling of turbidity currents on Navy Submarine Fan, California Continental Borderland. Sedimentology., 31, 169-185.

Canals, M., Puig, P., de Madron, X.D., Heussner, S., Palanques, A. and Fabres, J. (2006) Flushing submarine canyons. Nature., 444, 354-357.

Casalbore, D., Clare, M.A., Pope, E.L., Quartau, R., Bosman, A., Chiocci, F.L., Romagnoli, C. and Santos, R. (2020) Bedforms on the submarine flanks of insular volcanoes: New insights gained from high resolution seafloor surveys. Sedimentology.,

Cossu, R., Wells, M.G.and Wåhlin, A.K. (2010) Influence of the Coriolis force on the velocity structure of gravity currents in straight submarine channel systems. Journal of Geophysical Research: Oceans., 115.

Cossu, R. and Wells, M.G. (2013) The evolution of submarine channels under the influence of Coriolis forces: experimental observations of flow structures. Terra Nova., 25, 65-71.

Cossu, R., Wells, M.G. and Peakall, J. (2015) Latitudinal variations in submarine channel sedimentation patterns: the role of Coriolis forces. Journal of the Geological Society., 172, 161-174.

Covault, J. A., Kostic, S., Paull, C.K., Ryan, H.F. and Fildani, A. (2014) Submarine channel initiation, filling and maintenance from sea-floor geomorphology and morphodynamic modelling of cyclic steps. Sedimentology., 61, 1031-1054.

Covault, J.A., Kostic, S., Paull, C.K., Sylvester, Z. and Fildani, A. (2017) Cyclic steps and related supercritical bedforms: Building blocks of deep-water depositional systems, western North America. Marine Geology., 393, 4-20.

Ding, W,W., Li, J,B., Han, X.Q., Suess, E., Huang, Y.Y., Qiu, X.L. and Li, M.B. (2010) Morphotectonics and formation of the Taiwan Bank Canyon, southwest offshore Taiwan Island. Journal of Oceanography and Marine Science., 14, 65-78.

Ding, W.W., Li, J.B., Li, J., Fang, Y.X. and Tang, Y. (2013) Morphotectonics and evolutionary controls on the Pearl River Canyon system, South China Sea. Marine Geophysical Research., 34, 221-238.

Fildani, A., Normark, W.R., Kostic, S. and Parker, G. (2006) Channel formation by flow stripping: Large-scale scour features along the Monterey East Channel and their relation to sediment waves. Sedimentology., 53, 1265-1287.

Fonnesu, M., Palermo, D., Galbiati, M., Marchesini, M., Bonamini, E. and Bendias, D. (2020) A new world-class deep-water play-type, deposited by the syndepositional interaction of turbidity flows and bottom currents: The giant Eocene Coral Field in northern Mozambique. Marine and Petroleum Geology., 111, 179-201.

Gong, C.L., Wang, Y.M., Zhu, W.L., Li, W.G., Xu, Q. and Zhang, J.M. (2011) The Central Submarine Canyon in the Qiongdongnan Basin, northwestern South China Sea: architecture, sequence stratigraphy, and depositional processes. Marine and petroleum Geology., 28, 1690-1702.

Gong, C.L., Wang, Y.M., Peng, X.C., Li, W.G., Qiu, Y. and Xu, S. (2012) Sediment waves on the South China Sea Slope off southwestern Taiwan: implications for the intrusion of the Northern Pacific Deep Water into the South China Sea. Marine and Petroleum Geology., 32, 95-109.

Gong, C.L., Wang, Y.M., Zhu W.L., Li, W.G. and Xu, Q. (2013) Upper Miocene to Quaternary unidirectionally migrating deep-water channels in the Pearl River mouth Basin, northern South China Sea. AAPG bulletin., 97, 285-308.

Gong, C.L., Wang, Y.M., Xu, S., Pickering, K.T., Peng, X.C., Li, W.G. and Yan, Q. (2015) The northeastern South China Sea margin created by the combined action of down-slope and along-slope processes: Processes, products and implications for exploration and paleoceanography. Marine and Petroleum Geology., 64, 233-249.

Gong, C.L., Wang, Y.M., Rebesco, M., Salon, S. and Steel, R.J. (2018) How do turbidity flows interact with contour currents in unidirectionally migrating deep-water channels? Geology., 46, 551-554.

Hampton, M. A., Lee, H.J. and Locat, J. (1996) Submarine landslides. Reviews of geophysics., 34(1), 33-59.

He, Y., Zhong, G.F., Wang, L.L. and Kuang, Z.G. (2014) Characteristics and occurrence of submarine canyon-associated landslides in the middle of the northern continental slope, South China Sea. Marine and Petroleum Geology., 57, 546-560.

Heap, A. and Harris, P. (2008) Geomorphology of the Australian margin and adjacent seafloor. Australian Journal of Earth Sciences., 55, 555-585.

Hill, P., Moran, K. and Blasco, S. (1982) Creep deformation of slope sediments in the Canadian Beaufort Sea. Geo-Marine Letters., 2, 163.

Hsu, S.K., Yeh, Y.C., Doo, W.B. and Tsai, C.H. (2004) New bathymetry and magnetic lineations identifications in the northernmost South China Sea and their tectonic implications. Marine Geophysical Researches., 25, 29-44.

Keevil, G.M., Peakall, J. and Best, J.L. (2007) The influence of scale, slope and channel geometry on the flow dynamics of submarine channels. Marine and Petroleum Geology., 24, 487-503.

Kostic, S. (2014) Upper flow regime bedforms on levees and continental slopes, Turbidity current flow dynamics in response to fine-grained sediment waves. Geosphere., 10, 1094-1103.

Kuang, Z.G., Zhong, G.F., Wang, L.L. and Guo, Y.Q. (2014) Channel-related sediment waves on the eastern slope offshore Dongsha Islands, northern South China Sea. Journal of Asian Earth Sciences., 79, 540-551.

Lamb, M.P., Howard, A.D., Dietrich, W.E. and Perron, J.T. (2007) Formation of amphitheater-headed valleys by waterfall erosion after large-scale slumping on Hawai ‘i. Geological Society of America Bulletin., 119, 805-822.

Lamb, M.P., Parsons, J.D., Mullenbach, B.L., Finlayson, D.P., Orange, D.L. and Nittrouer, C.A. (2008) Evidence for superelevation, channel incision, and formation of cyclic steps by turbidity currents in Eel Canyon, California. Geological Society of America Bulletin., 120, 463-475.

Dantec, N. L., Hogarth, L.J., Driscoll, N.W., Babcock, J.M., Barnhardt, W.A. and Schwab, W.C. (2010) Tectonic controls on nearshore sediment accumulation and submarine canyon morphology offshore La Jolla, Southern California. Marine Geology., 268, 115-128.

Lee, S.E., Talling, P.J., Ernst, G.G. and Hogg, A.J. (2002) Occurrence and origin of submarine plunge pools at the base of the US continental slope. Marine Geology., 185, 363-377.

Lee, S.H. and Chough, S.K. (2001) High-resolution (2–7 kHz) acoustic and geometric characters of submarine creep deposits in the South Korea Plateau, East Sea. Sedimentology., 48, 629-644.

Li, X.Q., Fairweather, L., Wu, S.G., Ren, J.Y., Zhang, H.J., Quan, X.Y., Jiang, T., Zhang, C., Su, M., He, Y.L. and Wang, D.W. (2013) Morphology, sedimentary features and evolution of a large palaeo submarine canyon in Qiongdongnan basin, Northern South China Sea. Journal of Asian Earth Sciences., 62, 685-696.

Liao, W.Z., Lin, A.T., Liu, C.S., Oung, J.N. and Wang, Y. (2016) A study on tectonic and sedimentary development in the rifted northern continental margin of the South China Sea near Taiwan. Interpretation., 4, 47-65.

Liu, J.T., Kao, S.J., Huh, C.A. and Hung, C.C. (2013) Gravity flows associated with flood events and carbon burial: Taiwan as instructional source area. Annual Review of Marine Science., 5, 47-68.

Liu, Z.F., Zhao, Y.L., Colin, C., Stattegger, K., Wiesner, M. G., Huh, C. A., Zhang, Y.W., Li, X., Sompongchaiyakul, P. and You, C. F. (2016). Source-to-sink transport processes of fluvial sediments in the South China Sea. Earth-Science Reviews., 153, 238-273.

Masson, D., Howe, J. and Stoker, M. (2002) Bottom-current sediment waves, sediment drifts and contourites in the northern Rockall Trough. Marine Geology., 192, 215-237.

Meiburg, E. and Kneller, B. (2010). Turbidity currents and their deposits. Annual Review of Fluid Mechanics., 42, 135-156.

Micallef, A., Mountjoy, J. J., Canals, M. and Lastras, G. (2012) Deep-seated bedrock landslides and submarine canyon evolution in an active tectonic margin, Cook Strait, New Zealand. Submarine mass movements and their consequences., Springer, 201-212.

Micallef, A., Mountjoy, J.J., Barnes, P.M., Canals, M. and Lastras, G. (2014) Geomorphic response of submarine canyons to tectonic activity: Insights from the Cook Strait canyon system, New Zealand. Geosphere., 10, 905-929.

Miramontes, E., Eggenhuisen, J.T., Jacinto, R.S., Poneti, G., Pohl, F., Normandeau, A., CampbellF, D.C. and Javier Hernández-Molina, F. (2020) Channel-levee evolution in combined contour current–turbidity current flows from flume-tank experiments. Geology., 48(4), 353-357.

Mountjoy, J.J., Barnes, P.M. and Pettinga, J.R. (2009) Morphostructure and evolution of submarine canyons across an active margin: Cook Strait sector of the Hikurangi Margin, New Zealand. Marine Geology., 260, 45-68.

Nisbet, E.G. and Piper, D.J. (1998). Giant submarine landslides. Nature., 392, 329-330.

Normandeau, A., Campbell, D.C. and Cartigny, M.J.B. (2018) The influence of turbidity currents and contour currents on the distribution of deep-water sediment waves offshore eastern Canada. Sedimentology., 66, 1746-1767.

Normark, W.R., Piper. D.J., Posamentier. H., Pirmez, C. and Migeon S. (2002) Variability in form and growth of sediment waves on turbidite channel levees. Marine Geology., 192, 23-58.

Paull, C.K., Caress, D.W., Ussler, W., Lundsten, E. and Meiner-Johnson, M. (2011) High-resolution bathymetry of the axial channels within Monterey and Soquel submarine canyons, offshore central California. Geosphere., 7, 1077-1101.

Paull, C.K., Talling, P.J., Maier, K.L., Parsons, D., Xu, J.P., Caress, D.W., Gwiazda, R.,. Lundsten, E.M., Anderson, K. and Barry, J.P. (2018). Powerful turbidity currents driven by dense basal layers. Nature communications., 9, 1-9.

Piper, D.J.W. and Savoye, B. (1993) Processes of late Quaternary turbidity current flow and deposition on the Var deep-sea fan, north-west Mediterranean Sea. Sedimentology., 40, 557-582.

Piper, D.J.W. and Normark, W.R. (2009) Processes That Initiate Turbidity Currents and Their Influence on Turbidites: A Marine Geology Perspective. Journal of Sedimentary Research., 79, 347-362.

Pope, E., Talling. P.J, Urlaub. M., Hunt. J., Clare, M. and Challenor, P. (2015). Are large submarine landslides temporally random or do uncertainties in available age constraints make it impossible to tell? Marine Geology., 369, 19-33.

Pope, E. L., Jutzeler. M., Cartigny. M.J.B, Shreeve. J., Talling. P. J., Wright I.C. and Wysoczanski R.J. (2018) Origin of spectacular fields of submarine sediment waves around volcanic islands. Earth and Planetary Science Letters., 493, 12-24.

Pratson, L.F. and Coakley, B.J. (1996) A model for the headward erosion of submarine canyons induced by downslope-eroding sediment flows. Geological Society of America Bulletin., 108, 225-234.

Schnyder, J.S., Eberli, G.P., Betzler, C., Wunsch, M., Lindhorst, S., Schiebel, L., Mulder, T. and Ducassou, E. (2018) Morphometric analysis of plunge pools and sediment wave fields along western Great Bahama Bank. Marine Geology., 397, 15-28.

Sibuet, J.C., Hsu, S.K., Le Pichon, X., Le Formal, J.P., Reed, D., Moore, G. and Liu, C.S. (2002) East Asia plate tectonics since 15 Ma: constraints from the Taiwan region. Tectonophysics., 344, 103-134.

Sklar, L.S. and Dietrich, W.E. (2001) Sediment and rock strength controls on river incision into bedrock. Geology., 29, 1087-1090.

Stow, D.A., Faugères, J.C., Viana, A. and Gonthier E. (1998) Fossil contourites, a critical review. Sedimentary

Geology., 115, 3-31.

Symons, W.O., Sumner, E.J., Talling, P.J., Cartigny, M.J. and Clare, M.A. (2016). Large-scale sediment waves and scours on the modern seafloor and their implications for the prevalence of supercritical flows. Marine Geology., 371, 130-148.

Talling, P.J. Wynn, D., Masson, M., Frenz, B., Cronin, R., Schiebel., A., Akhmetzhanov, S., Dallmeier-Tiessen, S. and BenettiP, Weaver. (2007). Onset of submarine debris flow deposition far from original giant landslide. Nature., 450, 541-544.

Talling, P.J., Masson, D.G., Sumner, E.J. and Malgesini, G. (2012) Subaqueous sediment density flows: Depositional processes and deposit types. Sedimentology., 59, 1937-2003.

Taylor, B. and Hayes, D.E. (1983) Origin and history of the South China Sea basin. The tectonic and geologic evolution of Southeast Asian seas and islands: Part 2., 27, 23-56.

Wang, T.K., Chen, M.K., Lee, C.S. and Xia, K.Y. (2006) Seismic imaging of the transitional crust across the northeastern margin of the South China Sea. Tectonophysics., 412, 237-254.

Wang, K.L., Lo, Y.M., Chung, S.L., Lo, C.H., Hsu, S.K., Yang, H.J. and Shinjo, R. (2012) Age and Geochemical Features of Dredged Basalts from Offshore SW Taiwan: The Coincidence of Intra-Plate Magmatism with the Spreading South China Sea. Terrestrial, Atmospheric & Oceanic Sciences., 23.

Wang, X.X., Wang, Y.M., He, M., Chen, W.T., Zhuo, H.T., Gao, S.M., Wang, M.H. and Zhou, J.W. (2017) Genesis and evolution of the mass transport deposits in the middle segment of the Pearl River canyon, South China Sea: Insights from 3D seismic data. Marine and Petroleum Geology., 88, 555-574.

Williams, S.C.P. (2016) News Feature: Skimming the surface of underwater landslides. Proceedings of the National Academy of Sciences., 113, 1675-1678.

Wynn, R.B., Weaver, P.P., Ercilla, G., Stow, D.A. and Masson, D.G. (2000) Sedimentary processes in the Selvage sediment-wave field, NE Atlantic: new insights into the formation of sediment waves by turbidity currents.

Sedimentology., 47, 1181-1197.

Wynn, R.B. and Stow, D.A. (2002) Classification and characterisation of deep-water sediment waves. Marine Geology., 192, 7-22.

Xu, S., Wang, Y.M., Peng, X.C., Zou, H.Y., Qiu, Y., Gong, C.L. and Zhuo, H.T. (2014) Origin of Taiwan Canyon and its effects on deepwater sediment. Science China Earth Sciences., 57, 2769-2780.

Yeh, Y. C., Sibuet, J.C., Hsu, S.K. and Liu, C.S. (2010) Tectonic evolution of the Northeastern South China Sea from seismic interpretation. Journal of Geophysical Research: Solid Earth., 115.

Yin, S.R., Wang, L.L., Guo, Y.Q. and Zhong, G.F. (2015) Morphology, sedimentary characteristics, and origin of the Dongsha submarine canyon in the northeastern continental slope of the South China Sea. Science China Earth Sciences., 58, 971-985.

Yin, S.R., Lin, L., Pope, E. L., Li, J.B., Ding, W.F., Wu, Z., Ding, W.W., Gao, J. and Zhao, D.N. (2019) Continental slope-confined canyons in the Pearl River Mouth Basin in the South China Sea dominated by erosion, 2004–2018. Geomorphology., 344, 60-74.

Zhang, Y.W., Liu, Z.F., Zhao, Y.L., Colin, C., Zhang, X.D., Wang, M., Zhao, S.H. and Kneller, B. (2018) Long-term in situ observations on typhoon-triggered turbidity currents in the deep sea. Geology., 46, 675-678.

Zhao, F., Alves, T. M., Wu, S.G., Li, W., Huuse, M., Mi, L.J, Sun, Q.L. and Ma, B.J. (2016) Prolonged post-rift magmatism on highly extended crust of divergent continental margins (Baiyun Sag, South China Sea). Earth and Planetary Science Letters., 445, 79-91.

Zhao, Y.L., Liu, Z.F., Zhang, Y.W., Li, J.R., Wang, M., Wang, W.G. and Xu J.P. (2015) In situ observation of contour currents in the northern South China Sea: Applications for deepwater sediment transport. Earth and Planetary Science Letters., 430, 477-485.

Zhong, G.F., Cartigny, M. J., Kuang, Z.G. and Wang, L.L. (2015) Cyclic steps along the South Taiwan Shoal and West Penghu submarine canyons on the northeastern continental slope of the South China Sea. Bulletin., 127,

804-824.

FIGURES

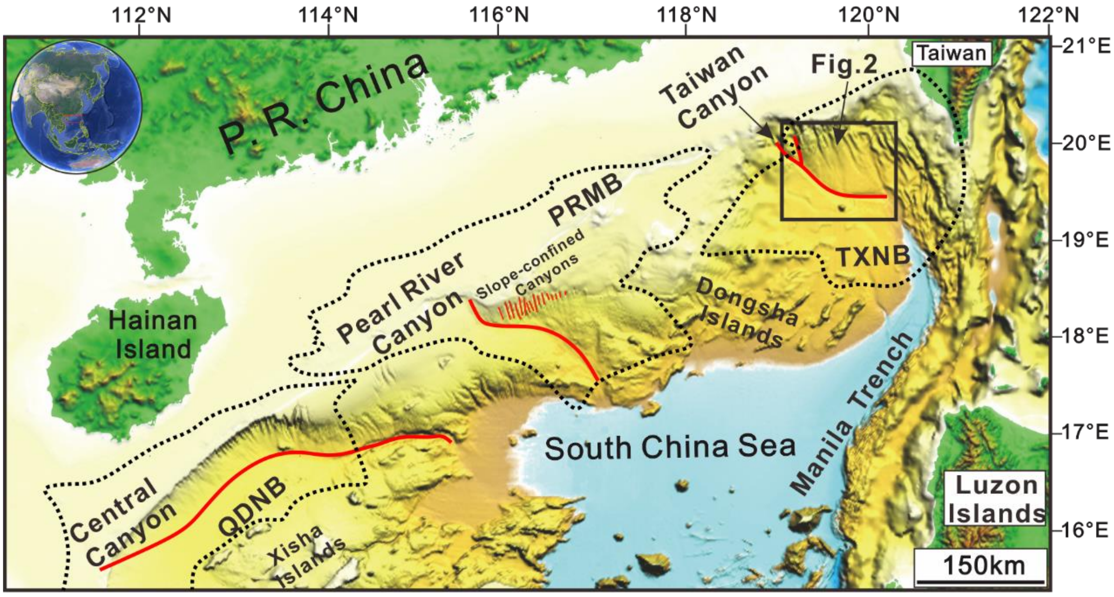

Fig. 1 Detailed location of the study area in the South China Sea. The red lines represent the Central Canyon, Pearl River Canyon, slope-confined canyons and Taiwan Canyon from southwest to northeast. The black box indicates the location of Fig. 2. The dashed black lines represent the boundaries of the Qiongdongnan Basin (QDNB), Pearl River Mouth Basin (PRMB) and Taixinan Basin (TXNB). Major topographical features such as the Xisha Islands, Dongsha Islands and Manila Trench, are highlighted in the figure.

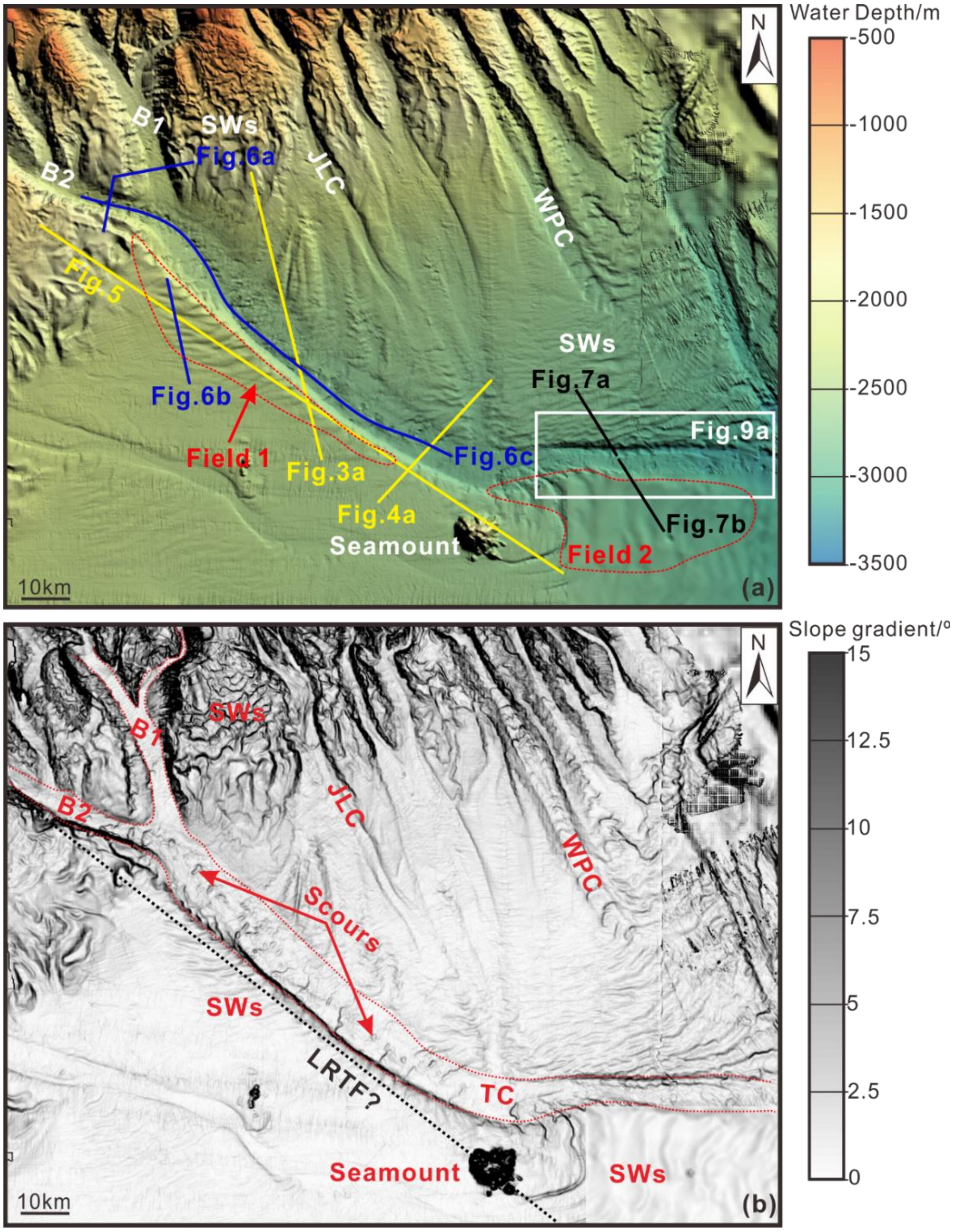

Fig. 2 (a) High-resolution multibeam bathymetric map of the study area showing several submarine canyons with large gullies in their heads. The white box represents the location of Figure 9a. The yellow solid line in the middle reach of Taiwan Canyon marks the location of the seismic profile in Figure 5. Two shorter yellow solid lines highlight the levee asymmetry of the Taiwan Canyon shown in Figures 3a and 4a. Three blue solid lines in the upper and middle reach of Taiwan Canyon represent seismic profiles shown in Figure 6a, b and c. (b) Slope gradient map of the study area. The black dotted line represents the potential location of Luzon-Ryukyu Transform Fault (LRTF). The red dotted lines indicate the rims of Taiwan Canyon. B1: Branch 1; B2: Branch 2; SW: sediment waves; TC: Taiwan Canyon; JLC: Jiulong Canyon; WPC: West Penghu Canyon.

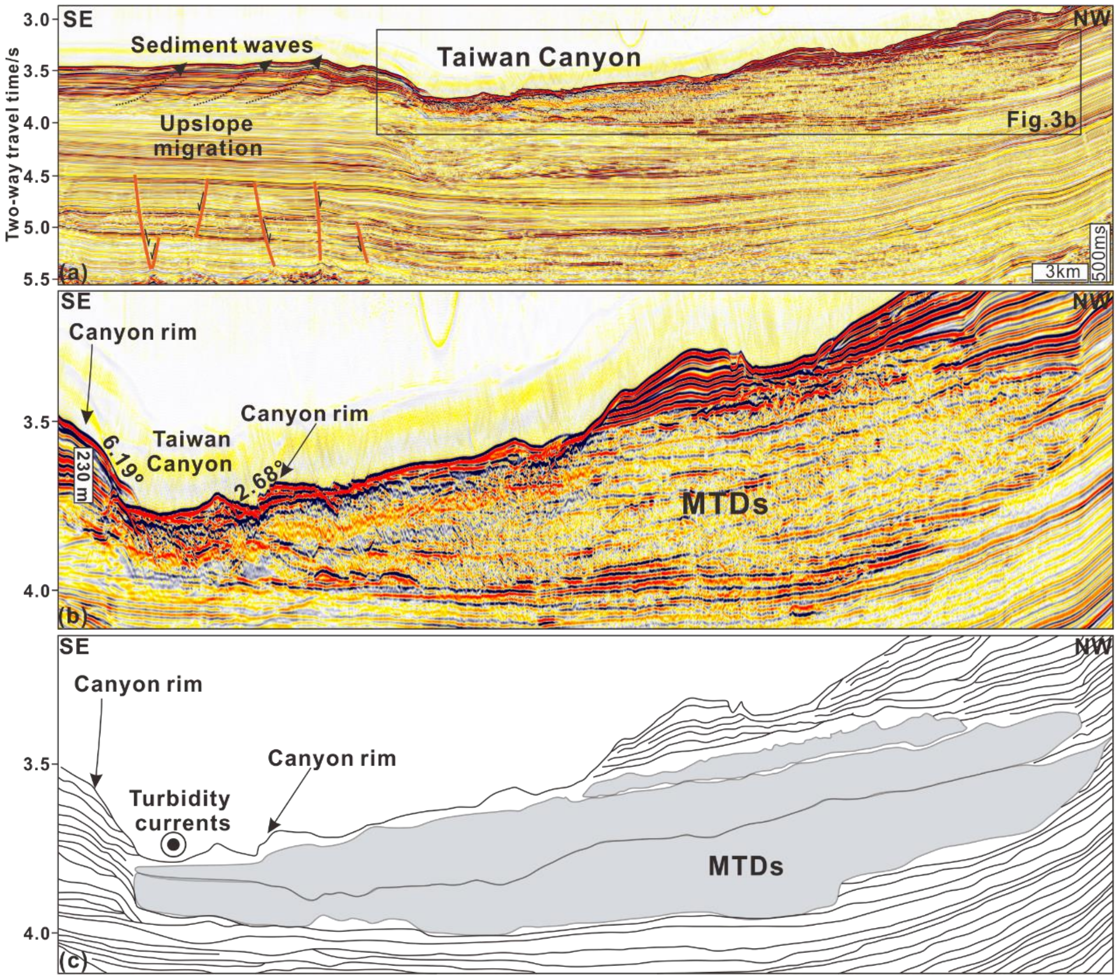

Fig. 3 (a) Two-dimensional (2D) seismic profile of the Taiwan Canyon highlighting the morphological differences in canyon banks shown in Figure 2. The black box indicates the location of the MTDs shown in Figure 3b. Note that slope gradient and the height of the southwest levee are larger than to the northeast. (b) The MTDs are characterized by chaotic amplitude reflections. The black arrows represent canyon rims. (c) Line-drawn interpretation of Fig. 3b illustrating the presence of widespread MTDs in the northeast of Taiwan Canyon. Note that the northeastern flank of Taiwan Canyon was eroded by these MTDs.

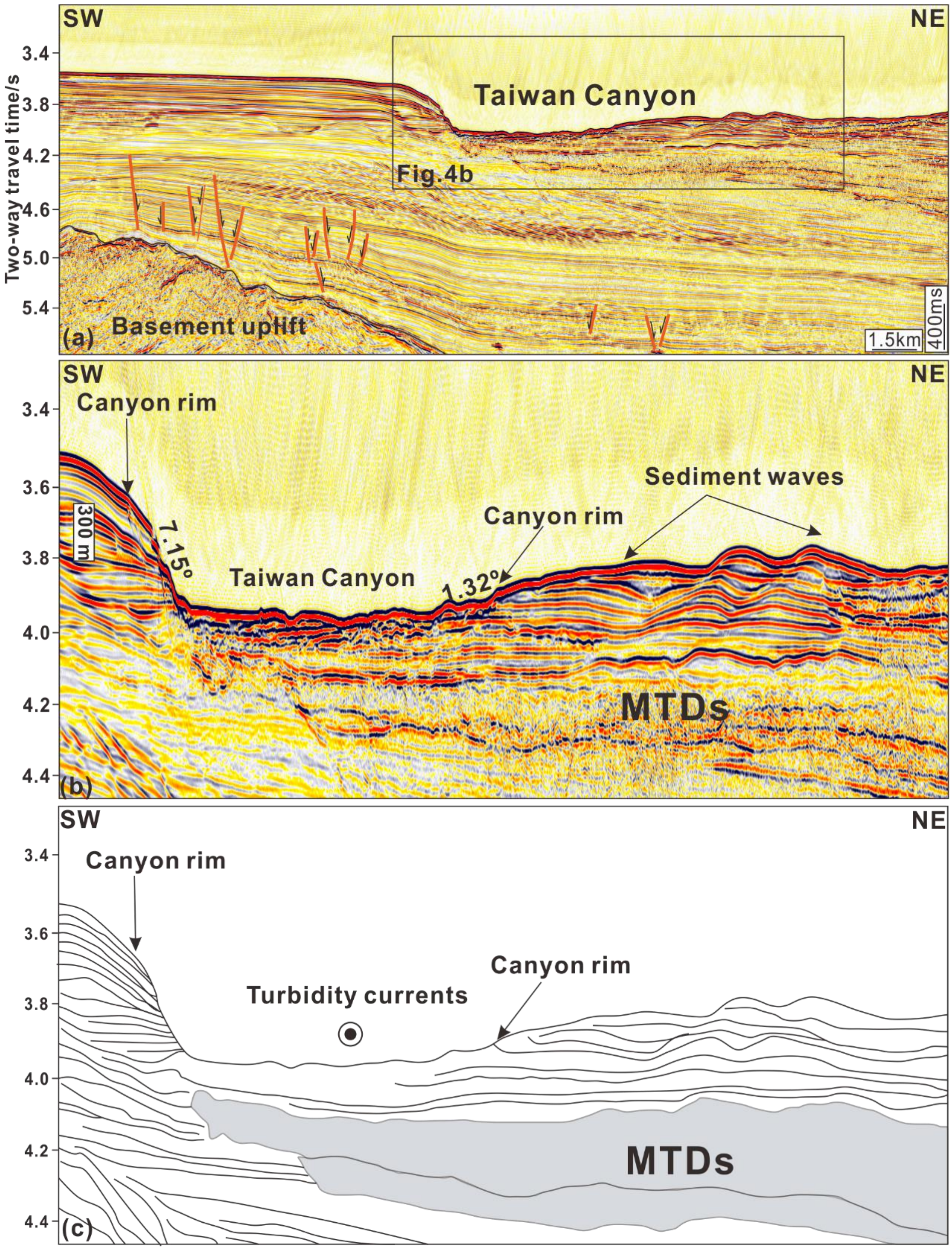

Fig. 4 (a) Two-dimensional (2D) seismic profile of the Taiwan Canyon showing the morphological differences in canyon banks imaged in Figure 2. The black box indicates the position of the MTDs shown in Figure 4b. (b) The MTDs are characterized by chaotic amplitude reflections. Note that slope gradient and the height of the southwest levee is larger than to the northeast. The black arrows point at canyon rims and sediment waves. (c) Line-drawn interpretation of Fig. 4b shows the internal architecture of the middle reach of Taiwan Canyon and numerous MTDs can be observed.

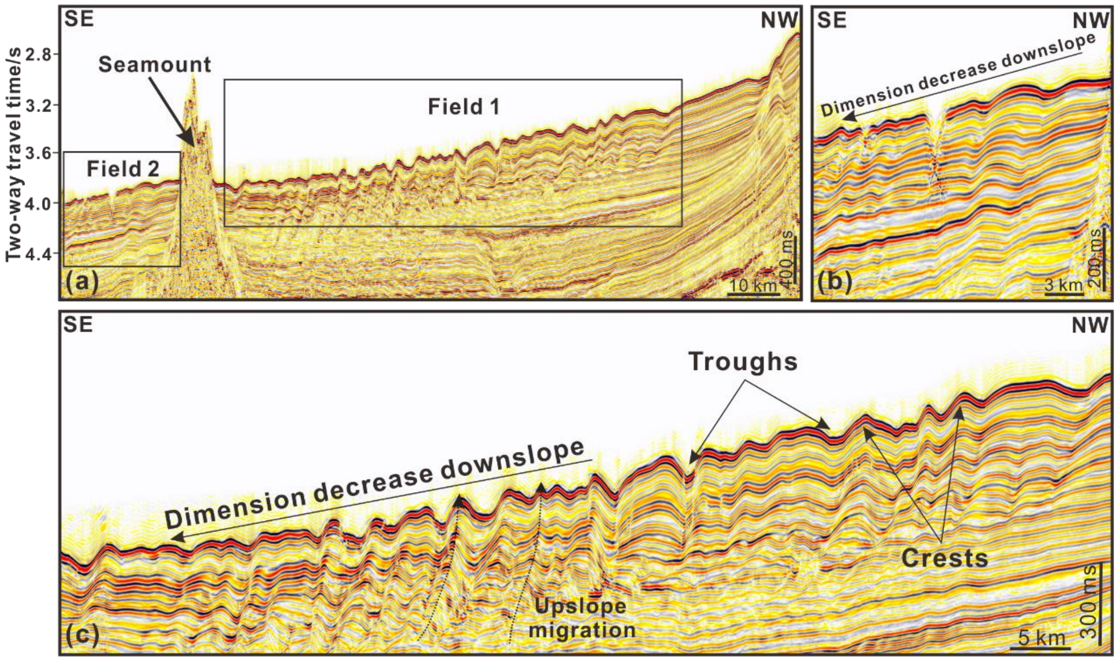

Fig. 5 (a) Two-dimensional (2D) multichannel seismic profile across an area with sediment waves in Fields 1 and 2 (see Figure 2 for location). The black box indicates the location of Fields 1 and 2 as shown in Figures 5c and 5b. (b) Upslope migration in sediment waves comprising Field 2. Downslope decrease is shown in the dimension of sediment waves in Field 2. (c) Upslope migration and downslope decrease of dimension in sediment waves comprising Field 1.

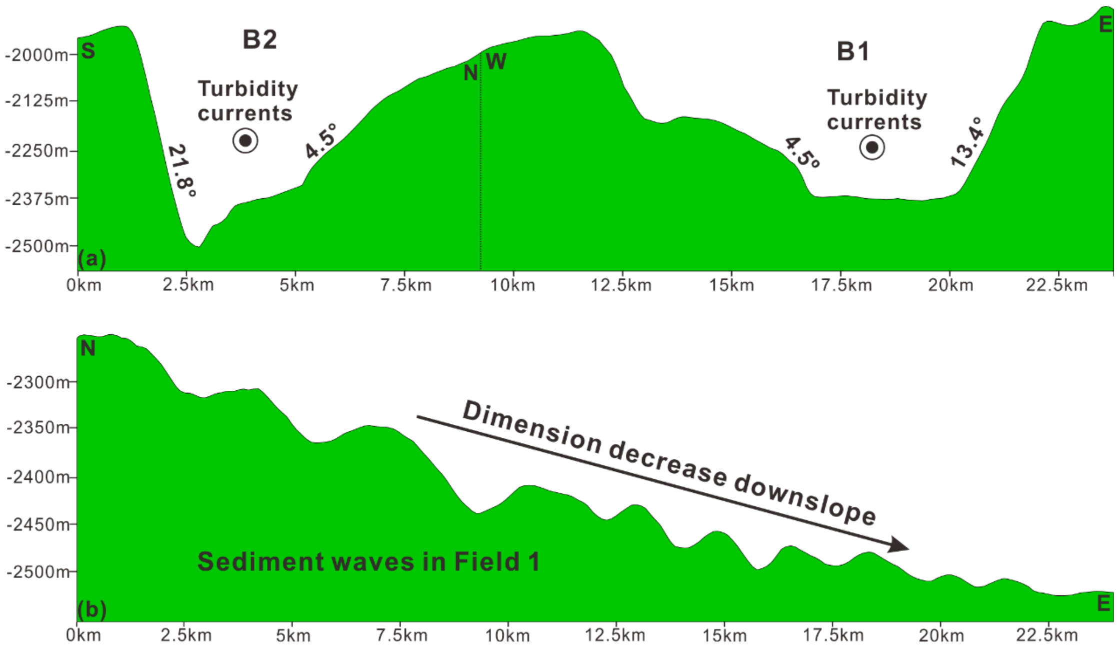

Fig. 6 (a) Bathymetric profile illustrating two branches (B1 and B2) in the upper reach of Taiwan Canyon. (b) Bathymetric profile showing the sediment waves in Field 1 and their dimensions (wavelengths and wave heights) decrease downslope.

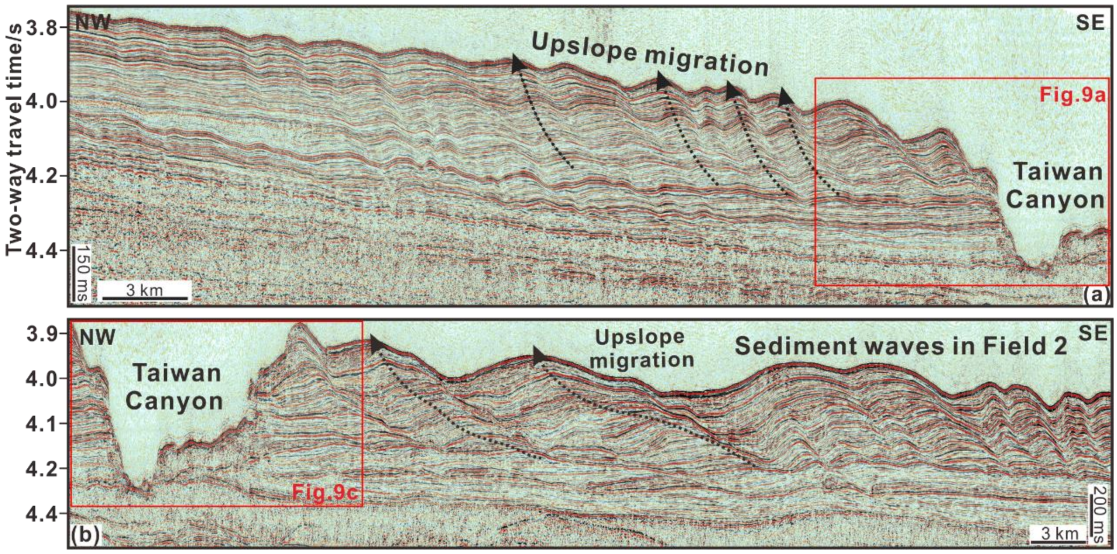

Fig. 7 (a) Two-dimensional (2D) multi-channel seismic profile of the seismic line modified from Gong et al. (2012). See Figure 2 for location. The red box indicates the trough (elongated depression) shown in Figure 9a. (b) 2D multi-channel seismic profile of the seismic line modified from Gong et al. (2012) in Figure 2. The red box indicates the trough shown in Figure 9c.

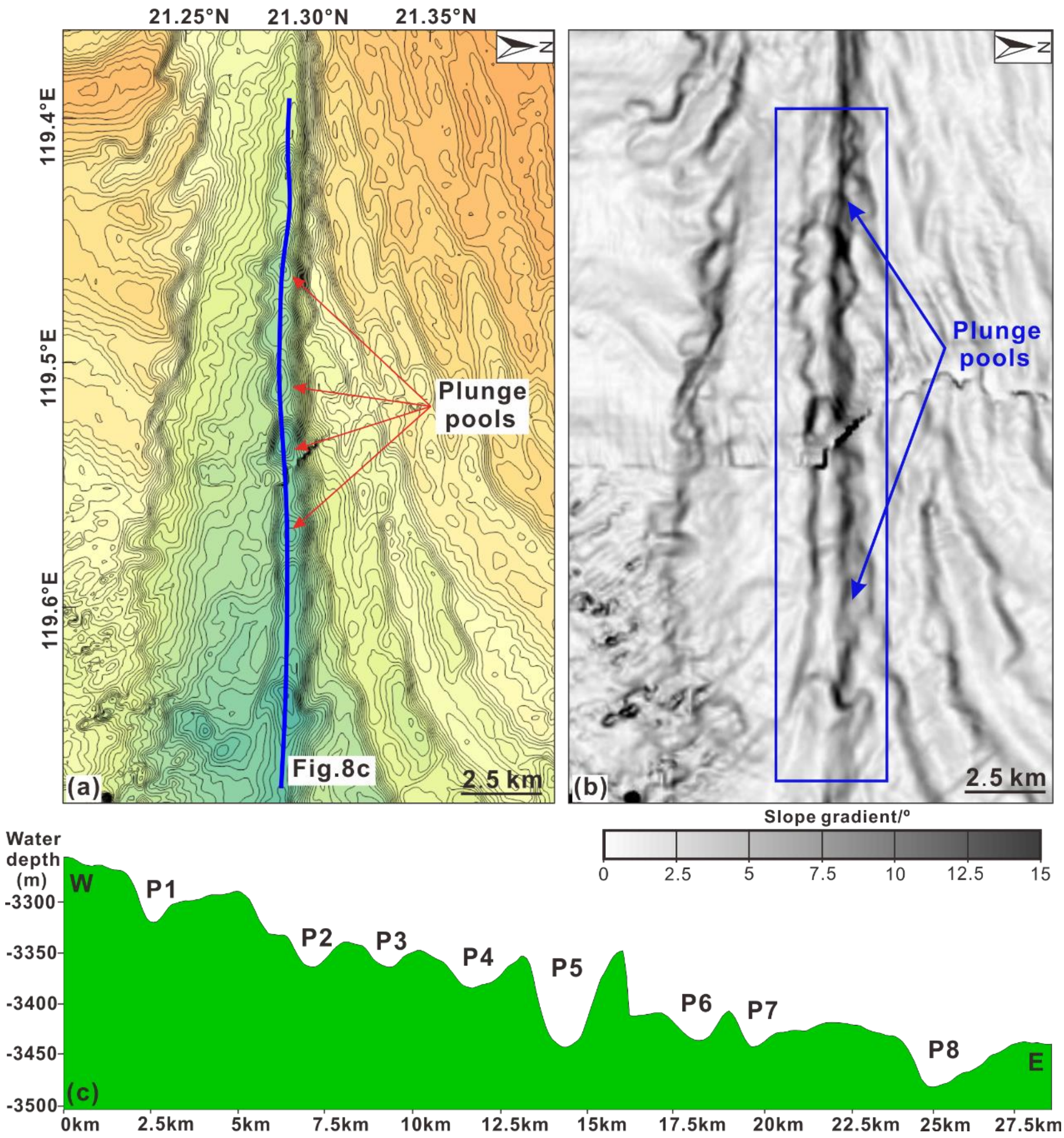

Fig. 8 (a) Contour map in the lower reach of Taiwan Canyon showing trains of plunge pools. The blue line indicates the cross-section profile of plunge pools shown in Figure 8c. (b) Slope gradient map illustrates the presence of numerous plunge pools within the trough. The blue box shows the distribution of plunge pools. (c) Cross-sectional bathymetric profile of the plunge pools shown in Figure 8a. Eight plunge pools are observed from the east to west at water depth from 3300 to 3500 m.

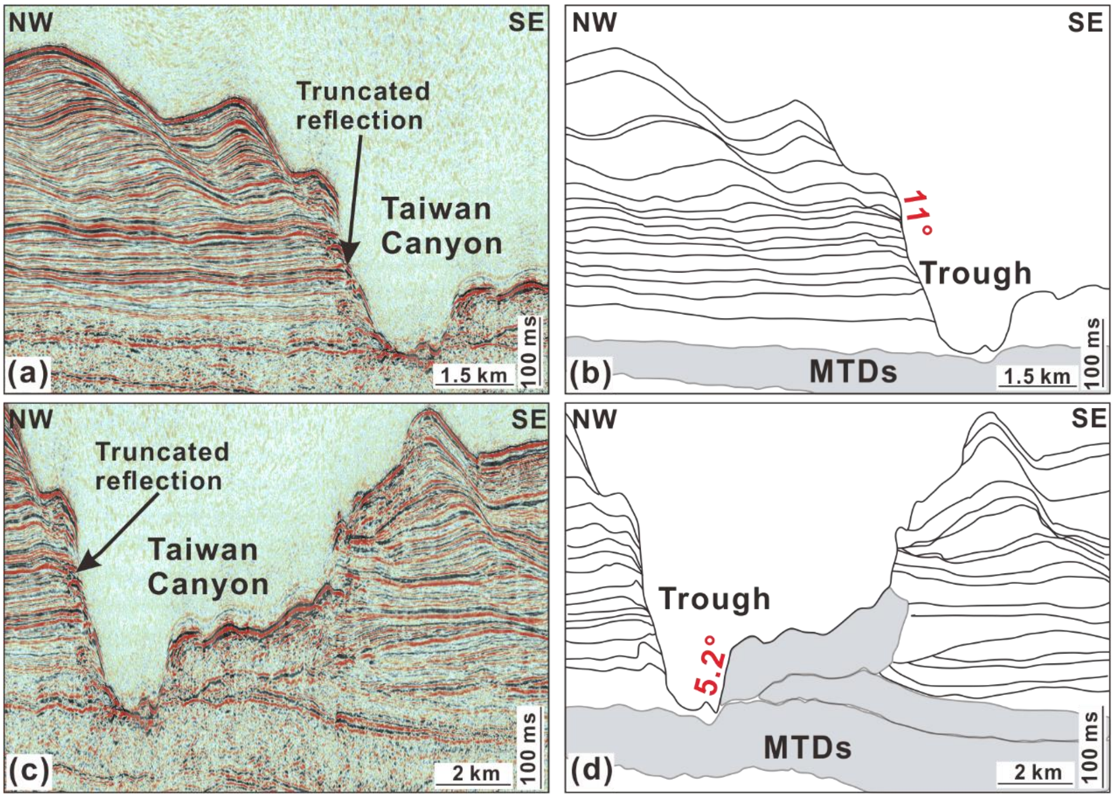

Fig. 9 (a) Two-dimensional (2D) multi-channel seismic profile of the trough in Figure 7a. Truncation reflections are observed on the seismic profile. Truncations can be observed on both sides of the trough. (b) Line-drawn interpretation of Fig. 9a outlining the internal architecture of trough and MTDs. (c) Two-dimensional (2D) multi-channel seismic profile of the trough shown in Figure 7b. Erosional truncation (truncated reflections) is observed on the seismic profile. (d) Line-drawn interpretation of Fig. 9c showing the internal character of trough at the bottom of Taiwan Canyon. The grey blocks indicate the recurrent MTDs.

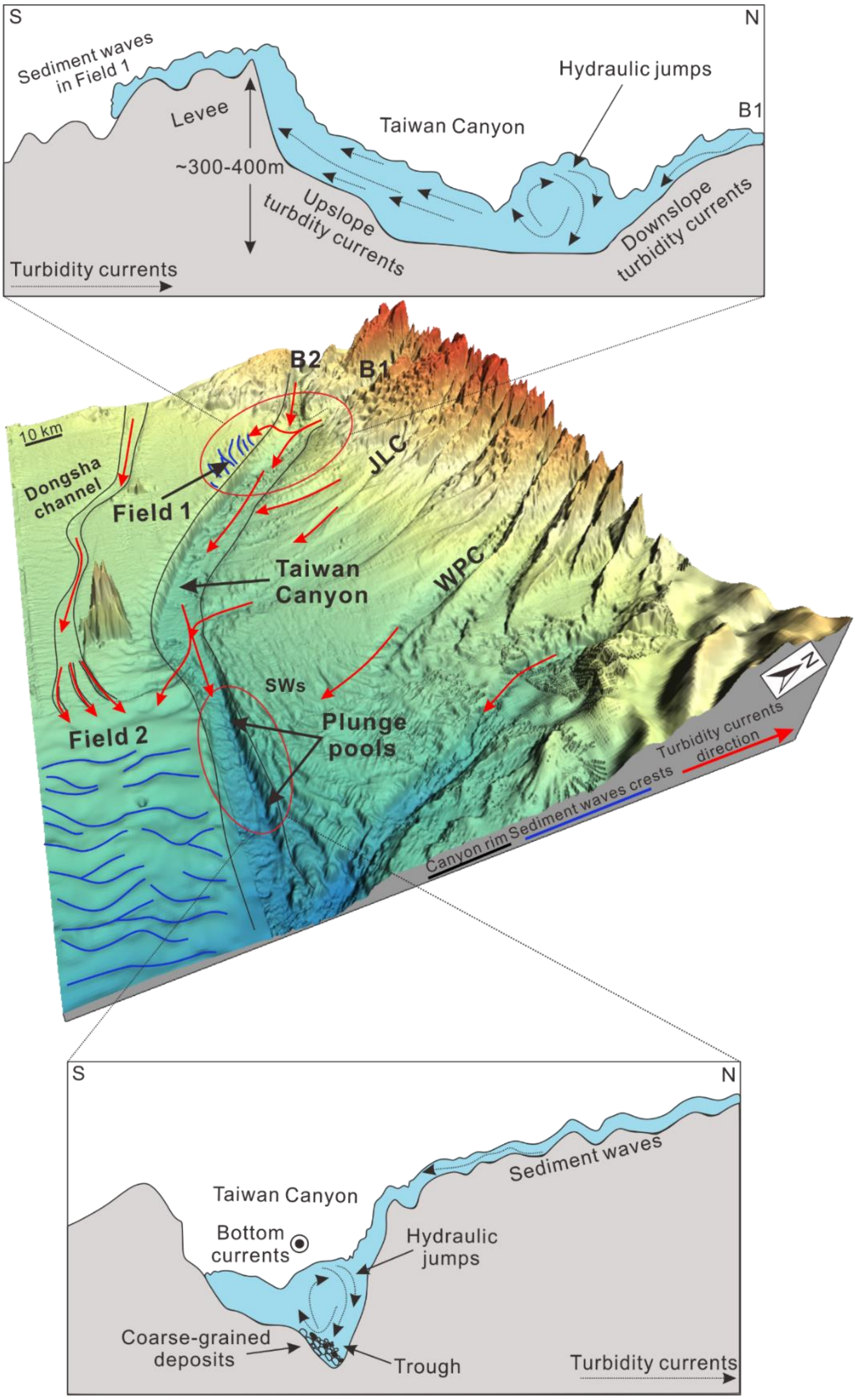

Fig. 10 Three-dimensional view of the morphological features within and around the Taiwan Canyon, including the sediment waves in Fields 1 and 2, and plunge pools in the lower reach of Taiwan Canyon. Schematic diagrams summarize the formation mechanisms of sediment waves in Field 1 and plunge pools in the lower reach of Taiwan Canyon. The dark grey lines indicate the position of the canyon rim, while the blue lines indicate the crests of sediment waves. The red arrows illustrate the direction of turbidity currents. B1: branch 1; B2: branch 2; SWs: sediment waves; JLC: Jiulong Canyon; WPC: West Penghu Canyon.